

Atomistically-informed solute drag in Al-Mg

F Zhang and W A Curtin

Division of Engineering, Brown University, Providence, RI 02912, USA

Abstract

Solute drag in solute-strengthened alloys, caused by diffusion of solute atoms around moving dislocations, controls the stress at deformation rates and temperatures useful for plastic forming processes. In the technologically-important Al-Mg alloys, the solute drag stresses predicted by classical theories are much larger than experiments. Here, the drag stress versus dislocation velocity is computed numerically using a realistic dislocation core structure to investigate the role of the core and obtain quantitative stresses for comparison to experiment. The model solves a discrete diffusion equation in a reference frame moving with the dislocation, with input solute enthalpies and diffusion activation barriers in the core computed atomistically. At low dislocation velocities, the solute drag stress is controlled by bulk solute diffusion because the core diffusion occurs too quickly. At intermediate velocities, both bulk and core diffusion can contribute to the drag, leading to a complex stress-velocity relationship showing two peaks in stress. At high velocities, the drag stress is controlled solely by diffusion within and across the core. At temperatures of 700K-750K typical of various Al-Mg processing methods, both mechanisms contribute over a range of practical strain rates. The drag stresses are much lower than predicted by continuum theories using a singular dislocation core but, in the low to intermediate velocity range, are comparable to values obtained by continuum models that use a Peierls-Nabarro model with a core spreading parameter tuned to best-match the atomistic models. Like the continuum models, the solute concentration dependence of the drag stress is nearly linear. Finally, the Orowan relationship is used to connect dislocation velocity to deformation strain rate. Accounting for the dependence of mobile dislocation density on stress, the simulations are in good agreement with recent experiments.

Keywords

aluminum alloys, solute diffusion, dynamic strain aging, dislocations

MSC:

Submitted to: Modelling and Simulation in Materials Science and Engineering

1. Introduction

The stress required to sustain a desired deformation rate, $\sigma(\dot{\epsilon})$, and the material strain rate sensitivity $m = d(\log(\sigma))/d(\log(\dot{\epsilon}))$ are critical constitutive relationships for the forming of metals in industrial applications. In various alloys at elevated temperatures, the phenomenon of “solute drag” due to diffusion of solutes toward moving dislocations can contribute to, and in some cases control, the strain rate sensitivity. The development of metal forming processes and the design of alloys for formability is therefore enhanced by mechanistic and predictive understanding of the stress/strain-rate dependence due to solute drag.

Solute strengthened materials can also exhibit dynamic strain aging (DSA) effects at lower temperatures, including the occurrence of negative strain rate sensitivity and undesirable instabilities in the form of Portevin-LeChatelier bands. The negative strain rate sensitivity is also generally attributed to solute diffusion toward dislocation cores. There are two prevailing concepts for the negative strain rate sensitivity. The dynamic view is that solute drag can only operate up to a critical velocity, beyond which the dislocation can escape the “cloud” of diffusion solutes and move much faster and at lower stresses. The prevailing view of the instability is that solutes collect around temporarily-pinned dislocations, necessitating larger applied stresses for the dislocations to escape the pinning sites. Recent interest in lightweight Aluminum alloys has sparked new work on continuum-level modeling of DSA and PLC effects [1,2], but the validity of such studies relies on a proper model for the underlying dynamical phenomena. A full picture of the dynamics of solute diffusion around dislocations, moving or pinned, is thus desirable for understanding DSA.

There is an extensive literature on modeling of DSA [3-14] and solute drag effects [15-21]. The analyses start from the relationship between the macroscopic shear strain rate $\dot{\gamma}$ and the dislocation velocity of dislocation v [22]

$$\dot{\gamma} = \rho_m b v, \quad (1)$$

where ρ_m is the density of mobile dislocation and b is the burgers vector. Models then address the dependence of dislocation velocity on stress and/or the evolution of the dislocation density with stress or strain.

The stress dependence of a dislocation moving at constant velocity in the presence of diffusing solutes, i.e. the solute drag problem, is well-established within a continuum framework [18] where the dislocation is modeled as a line defect with no core structure. The binding energy of a single solute at position (x, y) relative to a dislocation at the origin is given by to the work done by the solute misfit volume ΔV against the dislocation pressure field $p(x, y)$. For the continuum dislocation with a singular core, the binding energy is

$$H = p(x, y)\Delta V = \beta \frac{y}{x^2 + y^2} \quad ; \quad \beta = \frac{\mu b}{3\pi} \frac{1+\nu}{1-\nu} (v_s - v_a) \quad (2)$$

where μ is the shear modulus, ν the Poisson’s ratio, and v_s and v_a the atomic volumes of solute and host atoms, respectively. Assuming a solute diffusion coefficient $D_b = D_0 \exp\left(-\frac{H_b}{kT}\right)$,

where H_b is the activation enthalpy for bulk diffusion everywhere in the material, the drag stress on a dislocation moving at constant velocity is linear in the velocity at low stresses. The drag stress reaches a maximum at a critical velocity v_c given approximately as [15,16]

$$\tau_{\max} = 17c_0N\beta/b \text{ at } v_c \cong \frac{4D_b kT}{\beta}, \quad (3)$$

where N is the number of atoms per unit volume. These analytic results were subsequently verified by numerical studies [17] with dilute concentration solutes. Due to the singular pressure at the dislocation core and resulting divergence of the binding energy, a cut-off radius around the core is used in such analyses. In application to Al-Mg, the peak stress predicted by (3) is, however, orders of magnitude larger than experimental observations [23].

To avoid issues arising from a singular core and to approach realistic dislocation core structures, James [19] and James and Barnett [20] used the non-singular Peierls-Nabarro model for the dislocation pressure field, which leads to a solute binding energy of

$$H(x, y) = \beta \frac{y \pm \xi}{x^2 + (y \pm \xi)^2}, \quad (4)$$

where ξ is the half-width of the dislocation and the \pm term is positive for $y > 0$ and negative for $y < 0$. They also ensured site exclusion, leading to Fermi-Dirac rather than Boltzmann statistics, which was absent in the early models (although included in the simulations of Ref. [17]). James and Barnett [20] obtained a maximum stress significantly lower than (3) and having a strong dependence on the assumed dislocation half-width ξ . Taleff and Qiao [21] applied the James and Barnett model, with an assumed value for ξ , to investigate solute-drag creep in ternary Al alloys including Mg and Zn solutes and found results comparable to experimental data. Thus, elimination of the singular core and close attention to the statistical mechanics yields important corrections to the predicted drag stress, leading to closer agreement with experiments even though the model relies on a continuum dislocation pressure field even near the core.

Several recent works have begun analyzing the atomistic-scale interactions of Mg solutes in the cores of dislocations in Al. Picu and Zhang [24] calculated various activation energies for solute diffusion in Al-Mg alloy and showed notable differences as compared to the activation energy in bulk Al. Olmsted et al. studied the binding energy of Mg solutes in the atomistic core and showed that, even when the pressure field is manipulated to reasonably match the atomistic pressure field, the continuum solute binding energy is inaccurate in and just around the core. Xu et al. studied equilibrium solute clouds around a fixed dislocation using atomistic and kinetic Monte Carlo methods, and the effects of pre-existing solute clouds on the DSA [25,26]. Recognizing that the Mg diffusion rate in bulk Al away from the dislocation core is far too slow to account for dynamic strain aging effects observed around room temperature in Al-Mg, Curtin et al. [14] proposed a model in which it is only the Mg diffusion in the core of the dislocation, from the compression to tension side of the dislocation slip plane, that controls the strain aging. With all parameters obtained from atomistic simulations, they predicted the strengthening and strain rate range for DSA in good agreement with experimentally-deduced values. The detailed effects of the atomistic core structure, and phenomena such as the ‘‘cross-core’’ diffusion mechanism, on solute drag of moving dislocations have not yet been studied.

The objective of the present paper is to simulate solute drag using atomistic detail in the core and then to make specific predictions of solute drag stresses in Al-Mg as a function of dislocation velocity, temperature, and Mg concentration. We find that, at high temperatures where bulk diffusion can occur, the continuum models are reasonably accurate for Al-Mg over the range of dislocation velocities where deformation is usually performed, but that the treatment of the core influences the quantitative results and influences the drag at higher velocities. Our predicted solute drag stresses are consistent with experiments at $T=723\text{K}$. With decreasing temperature, the contributions to drag due to ‘‘bulk’’ and core regions become more distinct, being controlled by different activation energies for diffusion. Thus, in some materials, core-only solute diffusion may be dominant and cause drag stresses in regimes of temperature and/or strain rate at which bulk diffusion and standard solute drag models predict little or no drag stress.

The remainder of this paper is organized as follows. In Sec. 2, the theory for computing solute drag stress and the simulation of solute diffusion to obtain steady-state solute cloud distributions is described. In Sec. 3, we present the general predictions of the model for solute drag stresses as a function of velocity, temperature, and Mg concentration, compare to the prior theories, and discuss the factors controlling drag in different regimes. In Sec. 4, we use our computed results for drag stress versus velocity to compute the drag stress versus strain rate, and compare to the experimental data. We summarize our work in Sec. 5. The Appendix contains a derivation of the fundamental formula relating drag stress to the steady-state solute concentration.

2. Modeling of solute drag

2.1. General concepts and computational framework

The solute drag force is the force exerted by the solutes in the direction of dislocation motion. The relationship between the drag force and the solute binding energy $H(x, y)$ around the dislocation at the origin was given by Cottrell and Jaswon [15] and, for a dislocation gliding in the positive x direction, the corresponding drag stress is

$$\tau = \frac{F_x}{b} = -\frac{1}{b} \int_V cN \frac{\partial H}{\partial x} dV, \quad (5)$$

Cottrell and Jaswon did not derive (5), and the formula is widely quoted in the literature, so for completeness we provide a general derivation in Appendix A. Here, we model solute drag at the atomic scale, where atoms occupy discrete positions in space. The drag stress for the discrete problem is obtained from (5) by changing the integral to a discrete sum over atomic sites $\{i\}$ as

$$\tau = -\frac{1}{b} \frac{A}{v_s} \sum_i c_i \frac{dH}{dx}, \quad (6)$$

where c_i is the concentration at site i and A is the in-plane area occupied by one atom.

Eq. (6) shows that the solute drag stress can be computed given the steady-state solute concentration field around the moving dislocation. Here, we develop the general model for solute diffusion among discrete sites in an atomistic lattice containing a dislocation, closely paralleling Ref. [17]. The analysis is carried out with an atomic model of an edge dislocation. The dislocation is dissociated into two partials, and one partial and a segment of the stacking fault between the partials is shown in figure 1(a) when projected onto a 2d plane. For fcc materials, the distances between two atom positions along the x direction and y direction are $s = (1/2)(1/\sqrt{2})a$ and $t = 1/\sqrt{3}a$ respectively, where a is the lattice constant. The diffusion of a substitutional solute is mediated by vacancies in the crystal lattice, as reflected in the use of the activation energies associated that mechanism, and so explicit representation of the vacancies is unnecessary. Atomic jumps of the solute are considered to occur only between near-neighbor atom sites. Figure 1(b) shows a top view, looking down on the (111) dislocation glide planes, indicating the near-neighbor positions of any atom in the bulk lattice. There are six near-neighbors in the same glide plane at a distance equal to the burgers vector (shown in gray), three near-neighbors in a plane just above the chosen glide plane (shown in white), and three near-neighbor positions in a plane just below the chosen glide plane. In between the two partials, the structure changes due to the stacking fault but the number of neighbors in, above, and below the (111) plane remains the same. We will neglect, however, the changes in atomic coordination that occur right at the centers of the two partials, however. The solute atoms can jump to any of 12 near-neighbor positions and solute atoms on these 12 positions can jump into the central position. The diffusion between the central position and any of its neighbors depends on the concentrations of solute at these positions and the activation energy for motion between them. This is formalized by a discrete version of the diffusion equation. Consider site i surrounded by

neighbors $\{j=1, \dots, 12\}$. We denote the solute concentration as c_i and the activation energy barrier for solute motion from site i to site j as $Q_{i \rightarrow j}$. For a fixed dislocation, the rate of change of the concentration at site i is then

$$\frac{\partial c_i}{\partial t} = \sum_{j=1}^{12} \left[c_j (1 - c_i) \nu_0 \exp\left(-\frac{Q_{j \rightarrow i}}{kT}\right) - c_i (1 - c_j) \nu_0 \exp\left(-\frac{Q_{i \rightarrow j}}{kT}\right) \right]. \quad (7)$$

Here, ν_0 is the vibration frequency of the solute atom, and is related to the prefactor D_0 of the diffusion coefficient via $D_0 = 2\nu_0 b^2$ for fcc metals. If the dislocation is moving in the positive x direction with a velocity v then, in a reference frame that travels with the dislocation, the concentration at the nearest neighbor j_1 to the right (+ x) of site i moves into site i while the concentration at site i moves into the left neighbor $j_1(-x)$ of site i . Including this convection term and dividing by bulk diffusion coefficient D_b , we obtain

$$\begin{aligned} \frac{2b^2}{D_b} \frac{\partial c_i}{\partial t} = & \sum_{j=1}^{12} \left[c_j (1 - c_i) \exp\left(-\frac{Q_{j \rightarrow i} - H_b}{kT}\right) - c_i (1 - c_j) \exp\left(-\frac{Q_{i \rightarrow j} - H_b}{kT}\right) \right], \\ & + \frac{2b^2}{D_b} \frac{v}{s} (c_{j_1} - c_i) \end{aligned} \quad (8)$$

(8) is similar to the result of Ref. [17] but relevant for fcc materials. (8) is nearly a discrete version of the model of James and Barnett [20], but is slightly more general because diffusion across the glide plane in the core is included naturally and there is no assumption of slow variations in concentration that is implicit in the continuum diffusion equation.

An explicit fourth-order Runge-Kutta method is used to solve the set of coupled differential equations in (8). Because of the widely varying diffusion rates within the core versus outside the core (see below), a multi-time scale approach is used. Starting from a uniform solute concentration $c_i(t=0) = c_0$ for all sites i , at short times we solve (8) only in the core region. After each time increment, the maximum rate of concentration change in the core region is compared to that for diffusion to sites just outside the core region. When the maximum rate in the core region is 10 times faster than that just outside the core, we then begin to solve (8) over the entire model domain.

2.2. Activation energies for diffusion

The activation energies $Q_{i \rightarrow j}$ in (8) are the quantities that contain information about the local material structure. In general, considering two sites, the activation energies $Q_{i \rightarrow j}$ and $Q_{j \rightarrow i}$ between sites i and j are determined from the solute enthalpies at each site, H_i and H_j , and the migration enthalpy H_{ij} between them as

$$Q_{i \rightarrow j} = H_{ij} - H_i \quad ; \quad Q_{j \rightarrow i} = H_{ij} - H_j \quad . \quad (9)$$

At equilibrium, the transition rates are equal and the forms above guarantee that detailed balance is satisfied, i.e. $c_i / c_j = \exp[-(H_i - H_j) / kT]$.

Away from the dislocation core, the pressure field of the dislocation is small and varies slowly from site to site. The excess solute enthalpy is then taken to be identical to in form to that of the continuum model, i.e. $H_i = p(x_i, y_i) \Delta V$ as in (2). However, because the dislocation core in Al and other fcc metals is dissociated into partial dislocations, the pressure field is not given by

the standard continuum result. A good approximation to the atomistic-derived pressure field is obtained by spreading the core along the glide plane by discretizing the burgers vector into n equal increments located at atomic sites symmetrically distributed around the center of the dislocation [27]. We then use the continuum pressure field for each incremental burgers vector of magnitude b/n , and obtain

$$p(x_i, y_i) = -\frac{1+\nu}{3\pi(1-\nu)}\mu\frac{b}{n}\sum_{j=1}^n\frac{y_i}{(x_i-x_j)^2+y_i^2}, \quad (10)$$

where ν is Poisson's ratio. The migration enthalpy is then taken as the value for solute diffusion in the bulk material, $H_{ij} = H_b$. For Mg in Al, we use the values $H_b = 1.228\text{eV}$, $n = 12$, and $\nu_0 = 3.8 \times 10^{13} \text{ Hz}$.

Atomistic models show that the binding energy and diffusion activation energies for Mg in Al differ significantly from the continuum estimates given above in a narrow core region including two layers, one just above and one just below the dislocation slip plane, extending laterally just outside the positions of the two partial dislocations that bound the stacking fault region [14,24]. So although the discussion up until this point has been general, we now consider Al-Mg specifically. The Mg solute enthalpy H_i as a function of specific position i within the core was computed by Olmsted et al. [27] and we use those results. Diffusion is considered laterally along the layers above and below the glide plane, and also across the core between the tension and compression sides of the dislocation.

Diffusion laterally in the planes above and below the slip plane was studied by Picu and Zhang [24], who quote activation energies \bar{Q}^A and \bar{Q}^B for jumps in two directions for each atom position i as shown in figure 1(b) such that

$$Q_{i \rightarrow n4} = \bar{Q}_i^A, \quad Q_{i \rightarrow n2} = \bar{Q}_i^B. \quad (11)$$

Activation energies for jumps in the reverse directions and from all other surrounding neighbors were not directly provided. However, by symmetry along the dislocation line direction, jumps into sites $n6$ and $n5$ are equivalent to those for $n2$ and $n4$ respectively. Thus, we only need to determine the activation energies between site i and neighbors $n1$, $n2$, $n3$ and $n4$, which can be derived from the available Picu and Zhang data and the site enthalpies as follows. For diffusion between i and $n4$, (9) and (11) show that

$$\begin{cases} Q_{i \rightarrow n4} = H_{i,n4} - H_i = \bar{Q}_i^A \\ Q_{n4 \rightarrow i} = H_{i,n4} - H_{n4} \end{cases}. \quad (12)$$

from which we obtain

$$Q_{n4 \rightarrow i} = \bar{Q}_i^A + H_i - H_{n4}. \quad (13)$$

Similarly, the activation energies for diffusion between i and $n2$ are

$$\begin{cases} Q_{i \rightarrow n2} = \bar{Q}_i^B \\ Q_{n2 \rightarrow i} = \bar{Q}_i^B + H_i - H_{n2} \end{cases}. \quad (14)$$

The diffusion from i to $n1$ is similar to that from $n4$ to i and vice versa so that

$$\begin{cases} Q_{i \rightarrow n1} = \bar{Q}_{n1}^A + H_{n1} - H_i \\ Q_{n1 \rightarrow i} = \bar{Q}_{n1}^A \end{cases} \quad (15)$$

Similarly, the diffusion from i to $n3$ is similar to that from $n6$ to i and vice versa. Since diffusion between i and $n6$ is equivalent to that between i and $n2$ by symmetry along the dislocation line direction, the energies are

$$\begin{cases} Q_{i \rightarrow n3} = \bar{Q}_{n3}^A + H_{n3} - H_i \\ Q_{n3 \rightarrow i} = \bar{Q}_{n3}^A \end{cases} \quad (16)$$

(12)-(16) express all the activation energies for the diffusion in terms of migration enthalpies and solute enthalpies computed by Picu and Zhang [24] and Olmsted et al. [27].

For diffusion across the glide planes (“cross-core” diffusion), the migration enthalpy is taken to be $H_{ij}=0.97\text{eV}$ for all pairs of neighboring sites across the slip plane and between the cores of the two partials [24,27]. Data on site-specific cross-core migration enthalpies are not available. To make a smooth transition to the bulk migration enthalpy outside of the core along the slip plane, we assume H_{ij} to increase linearly up to the bulk value H_b over a distance $3.5b$ outside of the two partials, which is approximately one-half the partial spacing itself.

3. Result and Discussion

For results reported here, we use a system size $114 \times 184 \text{ \AA}$ containing $81 \times 80 = 6480$ atoms in two atomic planes through the thickness, due to symmetry. Periodicity in the through-thickness z -direction implies that the concentrations are only a function of the in-plane atom coordinates. This size encompasses the entire core and a sufficient number of “bulk” atoms to capture the solute concentration fields around moving dislocations at the velocities considered, as verified by computations using $161 \times 160 = 25,760$ atoms that show drag stresses differing by less than 0.5%. We study solute drag in Al-Mg at various temperatures and Mg concentrations, and necessary material parameters are listed in table 1.

Table 1. Material parameters for AA 5083 Al-Mg alloys.

$b(\text{m})$	c_0	$D_0 (\text{m}^2/\text{s})$	$H_b (\text{eV})$	$\mu(\text{GPa})$	ν	$v_s (\text{Mg})(\text{m}^3)$	$v_a (\text{Al})(\text{m}^3)$
2.85×10^{-10}	5 at%	7.72×10^{-7}	1.228	26	0.33	8.18×10^{-30}	1.41×10^{-29}

We first verify our numerical model and code by studying diffusion around the continuum singular dislocation core. Our results for the peak drag stress and other quantities are in good agreement with the results of Yoshinaga and Morozumi [17].

We next investigate the predictions of the discrete model of (8) using the Peierls-Nabarro core model and compare against the continuum model of James and Barnett. The discrete diffusion equation here is slightly different from the continuum model, and the differences should be negligible for dilute solute concentrations. We use the solute enthalpy from (4), a dislocation half-width of $\xi = 1.5b$, and the bulk migration enthalpy H_b and concentration $c_0=10$ at% as input to our model. Figure 2 shows the normalized drag stress $\frac{\tau}{\tau_0 c_0}$, where $\tau_0 = \frac{\beta}{v_a b}$, versus the

normalized dislocation velocity $\frac{v\beta}{D_b kT}$. Overall, the results of the two approaches are fairly

similar, but the discrete diffusion solution leads to higher drag stresses, about a factor of 2 at the peak, and a critical velocity about a factor of 2 larger as well. We must attribute these differences to two effects. First, the large concentration gradients that arise near the core region can make the

discrete diffusion equation more accurate than the continuum model. Second, the treatment of the cross-core diffusion is different in the two models, which could lead to differences as higher velocities are reached where the core region contributes to the drag.

We now investigate the influence of a realistic core structure for the dislocation. Details of the solute enthalpy and solute migration enthalpies for the Mg around the atomistic core of an Al edge dislocation were discussed in Section 2. To elucidate the role of the core, we study three different problems. The first problem is the “Full model” using the realistic core data of Section 2. The second problem is an “All Continuum” model in which the enthalpy is computed using the accurate continuum pressure field (equation (10)) and the bulk migration enthalpy everywhere including the core region. The third problem is a “P-N” model that uses an enthalpy derived from the Peierls-Nabarro pressure field everywhere (equation (4)), with $\xi=1.3b$ obtained by fitting to the accurate pressure field in the region around the dislocation, and the bulk migration enthalpy everywhere. Figure 3 shows the three solute enthalpy fields for the three problems, which are similar at moderate and far distances from the dislocation but different in detail near the dislocation. By adjusting the P-N parameter ξ , the P-N model (figure 3(c)) is in rough agreement with the accurate pressure field obtained by spreading the core (figure 3(b)) but differs in some detail. The results for drag stress versus velocity, normalized as noted before, are shown in figure 4. The agreement between the three models up to the peak stress is quite good, indicating that the drag up to the critical velocity is controlled mainly by the solute “cloud” that forms outside of the core region, where the pressure fields in all three models are quite similar. At low velocities, the drag stress scales linearly with the velocity, as expected.

Beyond the critical velocity, the “Full model” shows a different behavior than the usual models, including a second peak in the response and a final decrease at much higher velocities. These effects are entirely due to the drag contributions from diffusion in and around the core, which is much faster than the bulk diffusion. Analyzing the “Full model” in more detail, figure 5 shows the predicted drag stress versus dislocation velocity in dimensional units. The secondary peak stress is more clearly evident and the overall response suggests a sum of two separate mechanisms. To elucidate this further, figure 5 also shows the drag stress resulting from core diffusion (lateral and cross-core) only, obtained by setting the bulk migration enthalpy outside the core to infinity. The core-only response is basically similar in form to the usual continuum models – linear at low velocities, reaching a peak, and then falling off to zero – but shifted to higher velocity due to the faster core diffusion and with a peak drag stress determined by the core energetics. In the current Al-Mg simulations, the peak drag stress for the core-only diffusion is of the same order of magnitude as that from the bulk diffusion. In the standard continuum models, the contribution from the near-core region is typically assumed to be negligible compared to the contributions from outside the core [18], which is not the case here. The total drag stress is then approximately the sum of the stresses obtained from separate “bulk” and “core” mechanisms. We note that at low velocities, the core diffusion is too fast to contribute to the drag stress because the core concentration field is nearly in static equilibrium and symmetric around the dislocation core. In fact, the core drag stress has contributions from two different modes of diffusion, laterally along the glide planes and “cross-core”, but the activation energies are not sufficiently different to generate separate peaks in the drag stress versus velocity.

The discussion above is illuminated by examining the steady-state concentration fields around the moving dislocation core at various velocities. Figure 6 shows contours of the Mg concentration around the dislocation for several velocities corresponding to the points noted in figure 5. Figure 6(a) shows the equilibrium concentration for the static dislocation, which depends only on solute enthalpies and not on activation energies. The static solute “cloud” around the core is clearly evident but the excess concentration decreases steadily because the binding energy decreases and the temperature is fairly high. The concentration is symmetric about the center line and so cannot generate any drag stress. Figures 6(b)-(g) show the evolution of the cloud with increasing velocity. As the dislocation moves faster, the concentration field

becomes increasingly asymmetric and more localized around the core. At low velocities (figure 6(b) and 6(c)), the concentration field within the core remains nearly symmetric because the core diffusion is still near static equilibrium and the drag stress is controlled by the solute cloud outside of the core region. With increasing velocity, the excess concentration in the cloud decreases steadily, contributing to a decreasing drag, but the asymmetry in the distribution increases, contributing to increasing drag, with a net increase in drag stress. At the velocity corresponding to the peak drag stress (figure 6(d)), the effect of the decreasing concentration exceeds the effect of increasing asymmetry and the drag stress begins to decrease. Near the peak velocity, the concentration in the core begins to become asymmetric and thus begins to contribute to the drag stress. At higher velocities, the bulk diffusion cannot keep up with the dislocation and the solute cloud collapses into the core region (figure 6(e), (f)). At the second peak drag stress (figure 6(f)), the excess solute concentration is almost entirely contained within the two layers on either side of the slip plane, so that core diffusion becomes the only operative mechanism and controls the drag stress. The fast moving dislocation leaves a long narrow “tail” of excess concentration (excess on the tension side and depletion on the compression side) but examination of (6) easily shows that this cloud cannot contribute to a significant drag stress because it is gradients in the concentration profile along the x direction that control the drag stress and those gradients are small. At the highest velocities (figure 6(g)), the core diffusion is unable to keep up with the dislocation and the drag stress steadily decreases toward zero.

It is important to remark that in some materials it is quite possible that the bulk and core contributions to the drag could be more-widely separated in velocity, such that the observed drag stresses are entirely due to core effects. Thus, if quantitative measures of the drag stress are inconsistent with the standard continuum estimates, the core mechanism may be dominating the observed behavior.

The controlling mechanisms of deformation are also revealed through the temperature dependence of the drag stress. The drag stress versus velocity over the range $T=500\text{K}-800\text{K}$ is shown in figure 7 in log-log form. Although the temperature dependence of the continuum-only response can be scaled out as in figures 2 and 4, in the presence of bulk and core activation energies such a simple scaling does not exist. With decreasing temperature, and hence slower diffusion, the velocity range over which drag stresses are generated moves to slower velocities and the velocity regimes over which bulk and core diffusion contribute to the drag separate. Figure 7 shows that the velocity-stress relationship follows a power law with exponent of +1 in the low velocity regime and exponent of -1 in the high velocity regime. Analyzing the temperature dependence in these regimes reveals typical activation energies at low and high velocities, respectively, of

$$\bar{H}_{\text{low}} = 1.284\text{eV}; \quad \bar{H}_{\text{high}} = 0.910\text{eV}. \quad (17)$$

These values correspond reasonably closely to the activation energies for bulk diffusion (1.228eV) and cross-core diffusion ($\sim 0.90\text{eV}$ for diffusion from compression to tension), consistent with our prior discussion on the controlling mechanisms at low and high velocities.

Finally, figure 8 shows the normalized drag stress versus dislocation velocity as predicted for Al alloys with 0.1at%, 1at%, 3at% and 5at% Mg respectively at $T=723\text{K}$. The two peak drag stresses are attained at almost the same velocities independent of Mg solute concentration, confirming that the critical velocity is determined by the activation energy for the diffusion and independent about the concentration of the solute atoms. Furthermore, the peak stress varies nearly linearly with the solute concentration, as predicted by (3) for singular dislocation and as obtained by James and Barnett.

4. Comparison with the experiment

To make connections of our results to experiment requires converting dislocation velocities to appropriate strain rates. This is accomplished via the Orowan relation of (1) which involves the unknown dislocation density. Many previous investigations have, however, shown that the density of the mobile dislocation is also dependent on the shear stress [21,28-30], and several models motivate specific dependencies [28,29]. A common and model based on the general concept of internal stresses generated by dislocation-dislocation interactions is the Taylor model [28], which states that

$$\tau = \alpha \mu b \sqrt{\rho_m}, \quad (18)$$

where $\alpha \sim 0.3$ is an empirical coefficient [31]. Inverting (18) yields $\rho_m = (\tau / \alpha \mu b)^2$. Argon [29] suggests a similar square dependence of the density on shear stress. Substituting ρ_m from (18) into (1) yields a predicted strain-rate versus shear stress of

$$\dot{\gamma} = \left(\frac{\tau}{\alpha \mu b} \right)^2 b v(\tau). \quad (19)$$

In the linear regime of velocity versus stress $v(\tau) = B \tau$ with mobility parameter B , the strain rate is predicted to vary as the cube of the stress, i.e.

$$\dot{\gamma} = \alpha \mu B \left(\frac{\tau}{\alpha \mu b} \right)^3. \quad (20)$$

Within the above framework, we now compare the predictions of the current analysis with the work of Kulas et al. [23], who measured the shear-stress/strain-rate relationship on the Al-Mg system AA5083 containing 5at% Mg. For our comparisons, we select the data obtained for the coarser-grained specimen (sample DC-D-HB in Kulas et al.) at 723K, for which other deformation mechanisms such as grain boundary sliding are minimal. To make the comparison, the uniaxial tension stress σ and strain $\dot{\epsilon}$ measured by Kulas et al. are converted to shear stress τ and shear strain rate $\dot{\gamma}$ via the Taylor factor M in the standard way, $\tau = \frac{\sigma}{M}$ and $\dot{\gamma} = M \dot{\epsilon}$, with $M=3$ for an untextured fcc metal. Using the computed velocity/drag-stress relation $v(\tau)$ shown in figure 5, the results in figure 9 show excellent agreement with the experimental data using a value of $\alpha=0.322$, which is in the expected range. The model predicts a power law of close to 3 while the experimental data is closer to 4. As the peak stress is approached, the slope of $v(\tau)$ increases (figure 5), indicating that power laws greater than 3 can be achieved by the model. Nonetheless, the scaling is not in perfect agreement.

The model prediction shows unusual behavior once the drag stress begins to drop quickly. This regime of behavior should be considered with caution, since it is an unstable regime and since the use of the dislocation-density/stress relationship may fail in such regimes.

The data of Kulas et al. falls largely within the regime controlled by the bulk diffusion, so that the detailed core-diffusion effects studied here are not crucial. However, this agreement is obtained by using overall pressure and solute enthalpy fields that closely replicate the predictions from atomistic models. Thus, we believe the excellent agreement stems from using an accurate spread-core description. The only adjustable parameter in our model is then α , which is constrained to a fairly narrow range. This contrasts to prior models in which the dislocation core parameter ξ remains adjustable. Since the drag stress can vary dramatically with small variations in ξ [20], use of an accurate core model is essential for quantitative predictions.

We note that the realistic core structure used here comes from atomistic models using a particular Embedded Atom Method interatomic potential. This potential predicts a dislocation core spreading that is larger than expected to prevail in real Al. Recently, full quantum mechanical calculations of the structure of an Al core have been reported [32] showing that the spreading of the core in Al occurs over a distance of $\sim 8 \text{ \AA}$ rather than the $12\text{-}14 \text{ \AA}$ predicted by this EAM potential. Although not a large difference, the model predictions are sensitive to the core spreading. Hence, the close agreement with experiment achieved here could be fortuitous to some degree. Nonetheless, our results show that the core structure is important, and that solute behavior in the nanoscale region around a dislocation core can control macroscopic material deformation.

5. Conclusion

We have developed a numerical model for solute diffusion in a realistic, atomistically-informed, dislocation core so as to study the strain rate sensitivity of Al-Mg alloys in the high temperature solute drag regime. Although the work is closely related to earlier work by Yoshinaga and Morozumi and by James and Barnett, it is enhanced through the use of fundamental data from recent atomistic simulations. The model specifically includes solute enthalpies and diffusion in the core region of dislocation, which cannot be accurately predicted via standard continuum models for the solute enthalpy nor using bulk diffusion coefficients. The simulation results show the expected low-velocity regime where $\tau \approx v$ as controlled largely by solute diffusion outside of the immediate core. Continuum models using an appropriately-chosen core spreading parameter can show good quantitative agreement with the complete model in this regime. At larger velocities, the diffusion and enthalpies in the core region contribute to the drag stress, and ultimate control the drag stress at very high velocities. Although not occurring in Al at typical processing temperatures, the core-controlled drag stresses could be important in other materials. Application of the realistic model to Al-Mg alloys shows quantitative agreement with experiments which, although within the low velocity regime, demonstrates that inclusion of the detailed core spreading to capture the solute enthalpy outside of, but nearby, the core can make the models predictive. We envision extension of the work here to the study of other solute additions to Al, such as Zn as done by Taleff et al. and broader application to other materials systems where the solute drag mechanism is used to control deformation rates in material forming.

Acknowledgement

This work was supported by General Motors at Brown University as part of the GM-Brown Collaborative Research Laboratory on Computational Materials Science.

Appendix A.

For an edge dislocation of unit length, the drag stress is determined by $\tau = \frac{F}{b}$ where F is the total drag force on the moving dislocation. The dragging force F_a on one atom at a drift velocity v_D is related to the mobility D/kT by the Einstein mobility relation [33]

$$\mathbf{F}_a = \frac{\mathbf{v}_D}{(D/kT)}. \quad (\text{A.1})$$

where \mathbf{F}_a and \mathbf{v}_D are vectors for the 3-dimensional case. When the cloud of the solute atoms around a moving dislocation attains a steady-state configuration, the drag can be viewed as a group of excess solute atoms traveling with the moving dislocation at the same velocity, i.e., $\mathbf{v}_D = \mathbf{v}$, while other solute atoms remain fixed. The total drag force is then the sum of the forces exerted by each of the excess atoms in the cloud [18], given by

$$\mathbf{F} = \sum \frac{kT}{D} \mathbf{v} = kT \mathbf{v} \int_V \frac{1}{D} (c - c_0) N dV . \quad (\text{A.2})$$

c is the spatially-varying concentration of solute atoms. (A.2) is simple and expresses the physical meaning clearly, but is difficult to use because the solute cloud may have a long tail emanating from the back end of the moving dislocation core that then requires considering a large integration volume. We thus pursue a different approach to compute \mathbf{F} in an efficient and accurate manner, as follows.

The flux \mathbf{J} of the solutes is given by Fick's law with an additional drift current,

$$\mathbf{J} = -DN\nabla c + c\mathbf{v}_D . \quad (\text{A.3})$$

The drift velocity \mathbf{v}_D is determined by the Einstein mobility relation using the force $\mathbf{F} = -\nabla H$ produced by the dislocation/solute interaction energy H , so that

$$\mathbf{J} = -DN\nabla c - cN \frac{D}{kT} \nabla H . \quad (\text{A.4})$$

Mass conservation equation further requires that

$$-N \frac{\partial c}{\partial t} = \nabla \cdot \mathbf{J} . \quad (\text{A.5})$$

In a coordinate system moving at constant velocity \mathbf{v} , the accumulation term is $-\partial c / \partial t = \mathbf{v} \cdot \nabla c$ [18] and $\mathbf{v} \cdot \nabla c = \nabla \cdot (\mathbf{v}c)$. Substituting into (A.5), the conservation equation then becomes

$$N\nabla \cdot (\mathbf{v}c) = \nabla \cdot \mathbf{J} . \quad (\text{A.6})$$

which is integrated directly to yield

$$-\mathbf{J} + \mathbf{v}(c - c_0)N = \mathbf{0} , \quad (\text{A.7})$$

leading to

$$D\nabla c + c \frac{D}{kT} \nabla H + \mathbf{v}(c - c_0) = \mathbf{0} \quad (\text{A.8})$$

Dividing (A.8) by D/kT and integrating over the whole volume V the system gives

$$kT \int_V DN\nabla c dV + \int_V cN\nabla H dV + kT \mathbf{v} \int_V \frac{1}{D} (c - c_0) N dV = \mathbf{0} . \quad (\text{A.9})$$

The first term is eliminated by divergence theorem,

$$kT \int_V DN\nabla c dV = kT \int_{\Omega} DcN d\mathbf{A} = kTND_b c_0 N \int_{\Omega} d\mathbf{A} = \mathbf{0} , \quad (\text{A.10})$$

where Ω is the boundary surface of the object and D_b is the value of D for the bulk diffusion far from the dislocation. The last term in (A.9) is the force \mathbf{F} , yielding the final result

$$\mathbf{F} = - \int_V cN\nabla H dV . \quad (\text{A.11})$$

Because the interaction potential decays quickly away from the dislocation, the integration in (A.11) can be performed on a relatively small region. Choosing the dislocation to move along the x direction leads to the result quoted in (5) of the text.

References

- [1] Lasko G, Hahner P and Schmauder S 2005 *Model. Simul. Mater. Sc.* **13** 645-56
- [2] Hopperstad O S, Borvik T, Berstad T, Lademo O G and Benallal A 2007 *Model. Simul. Mater. Sc.* **15** 747-72
- [3] Cottrell A H and Bilby B A 1949 *Proc. Phys. Soc. A* **62** 49-62
- [4] Penning P 1972 *Acta Metall.* **20** 1169-75
- [5] McCormick P G 1972 *Acta Metall.* **20** 351-54
- [6] Van den Beukel A 1975 *Phys. Status Solidi A* **30** 197-206
- [7] Louat N 1981 *Scripta Metall.* **15** 1167-70
- [8] Estrin Y and Kubin L P 1989 *J. Mech. Behav. Mater.* **2** 255-92
- [9] Kubin L P and Estrin Y 1992 *Phys. Status Solidi B* **172** 173-85
- [10] Zhang S, McCormick P G and Estrin Y 2001 *Acta Mater.* **49** 1087-94
- [11] Kok S, Bharathi M S, Beaudoin A J, Fressengeas C, Ananthakrishna G, Kubin L P and Lebyodkin M 2003 *Acta Mater.* **51**, 3651-62
- [12] Picu R C 2004 *Acta Mater.* **52** 3447-58
- [13] Fressengeas C, Beaudoin A J, Lebyodkin M, Kubin L P and Estrin Y 2005 *Mat. Sci. Eng. A* **400-401** 226-30
- [14] Curtin W A, Olmsted D L and Hector L G 2006 *Nat. Mater.* **5** 875-80
- [15] Cottrell A H and Jaswon M A 1949 *P. Roy. Soc. Lond. A* **199** 104-14
- [16] Cottrell A H 1953 *Dislocations and Plastic Flow in Crystals* (Oxford: Clarendon)
- [17] Yoshinaga H and Morozumi S 1971 *Philos. Mag.* **23** 1367-85
- [18] Hirth J P and Lothe J 1982 *Theory of Dislocations* 2nd Ed. (New York: John Wiley & Sons)
- [19] James W L 1986 *A Re-Examination of the Solute Drag Force on a Gliding Edge Dislocation* Ph. D. Thesis (Stanford CA: Stanford University)
- [20] James W L and Barnett D M 1986 A re-examination of atmospheres and impurity drag on moving dislocations *Solute-Defect Interaction: Theory and Experiment: Proc. of the International Seminar (Kingston, Canada, 5-9 August 1985)* ed S Saimoto et al (Toronto: Pergamon) pp 136-42
- [21] Taleff E M and Qiao J 2001 Numerical modeling of solute-drag creep. *Modeling the Performance of Engineering Structural Materials II: 2001 TMS Fall Meeting (Indianapolis, IN, 4-8 November)* ed D R Lesuer and T S Srivatsan (Warrendale, PA: TMS) pp 3-12
- [22] Orowan E 1940 *Proc. Phys. Soc.* **52** 8-22
- [23] Kulas M A, Green W P, Taleff E M, Krajewski P E and McNelley T R 2005 *Metall. Mat. Trans A*, **36A**, 1249-61
- [24] Picu R C and Zhang D 2004 *Acta mater.* **52** 161-71
- [25] Xu Z and Picu R C 2006 *Model. Simul. Mater. Sc.* **14**, 195-206
- [26] Xu Z J and Picu R C 2007 *Model. Simul. Mater. Sc.* **15**, 385-96
- [27] Olmsted D L, Hector L G and Curtin W A 2006 *J. Mech. Phys. Solids* **54** 1763-88
- [28] Taylor G I 1934 *P. Roy. Soc. Lond. A* **145** 362-87
- [29] Argon A S 1970 *Scripta Metall.* **4** 1001-04
- [30] Frost H J and Ashby M F 1982 *Deformation-Mechanism Maps* (Oxford, New York: Pergamon)
- [31] Ashby M F 1970 *Phil. Mag.* **21** 399-424.
- [32] D. Trinkle, L. G. Hector, C. Woodward, D. Olmsted. Accurate prediction of dislocation core in Aluminum Submitted to *Phys. Rev. Lett.*
- [33] Shewmon P G 1963 *Diffusion in Solids* (New York: McGraw-Hill)

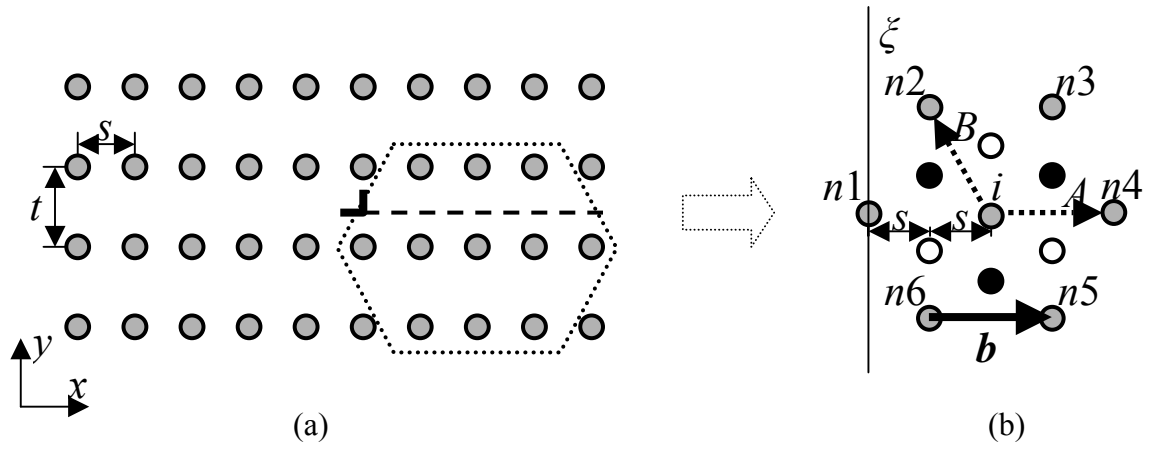


Figure 1. Atom structure around one partial of an edge dislocation: (a) Side view with dislocation line perpendicular to the plane of view; (b) Top view of atoms positions around a central atom position. The dislocation line (ζ) and the Burgers vector (\mathbf{b}) are also shown, as well as notation used in the text.

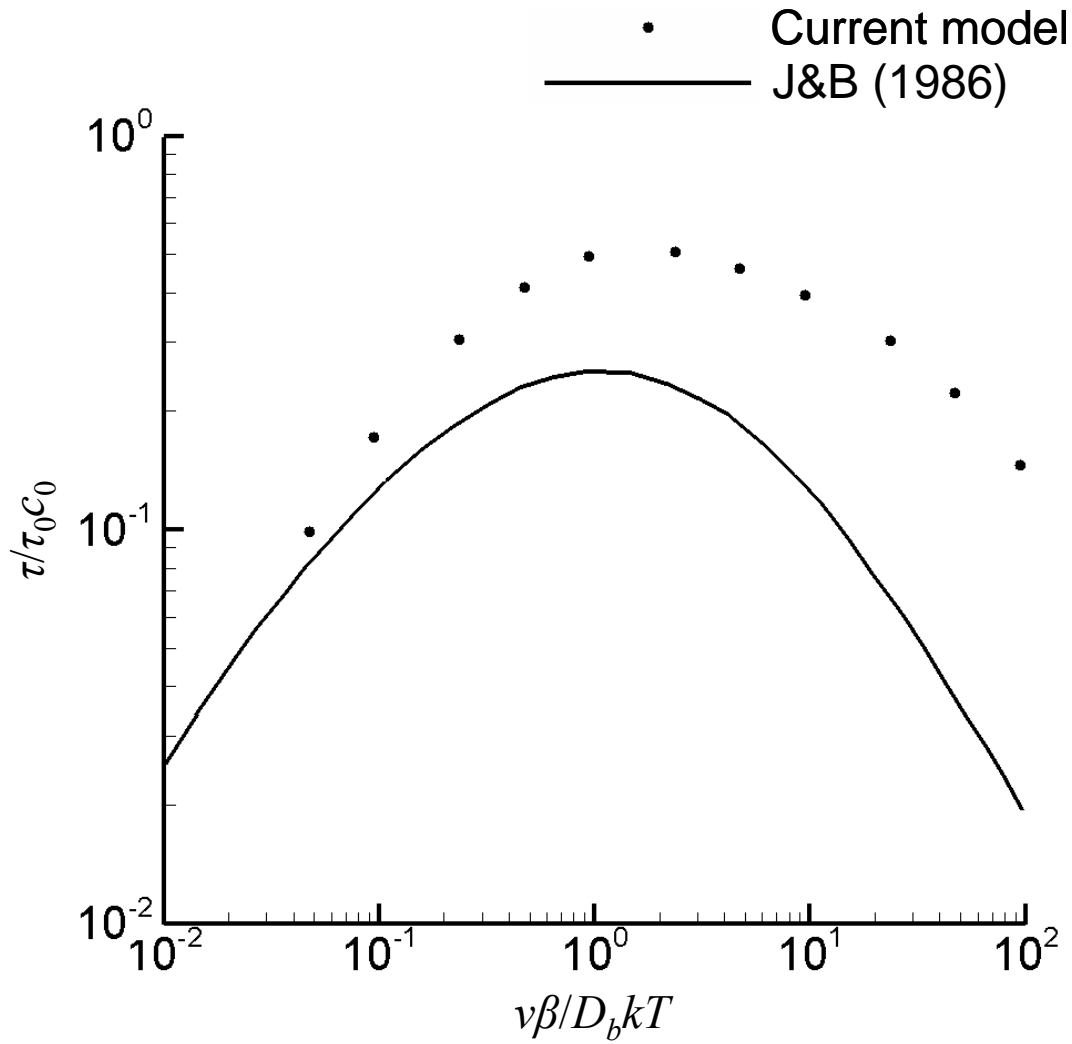


Figure 2 Normalized drag stress versus normalized velocity, as predicted by the present model (points) and by James and Barnett [20] for a Peierls-Nabarro core model with dislocation half-width of $\zeta = 1.5b$ at $c_0 = 10$ at% Mg.

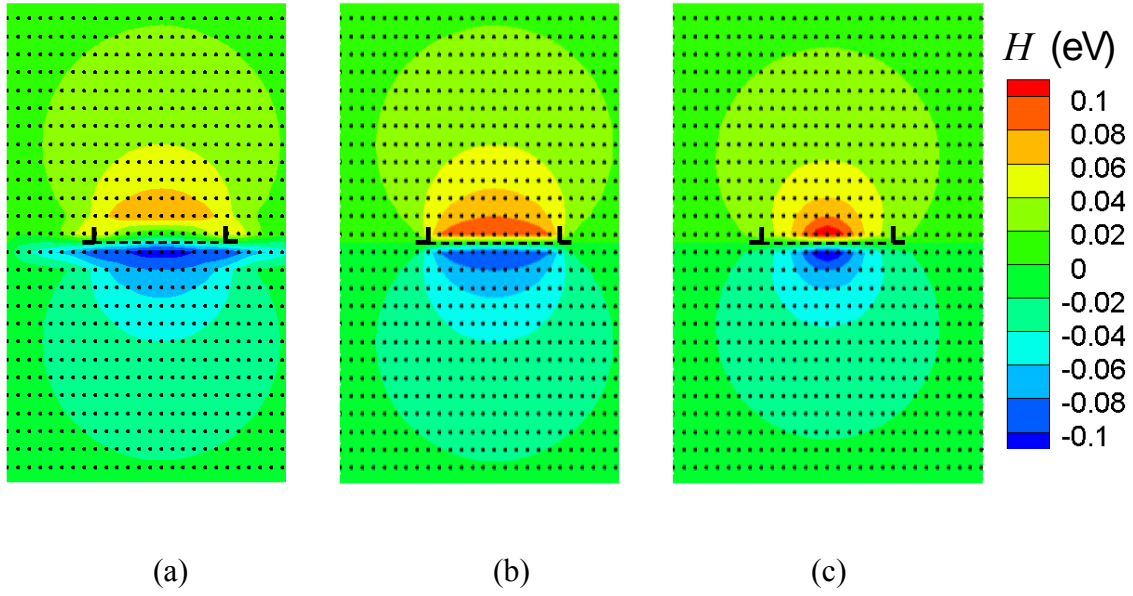


Figure 3. Comparison of the enthalpy field between (a) ‘Full model’, (b) ‘All continuum’ model, and (c) PN model with $\xi = 1.3b$.

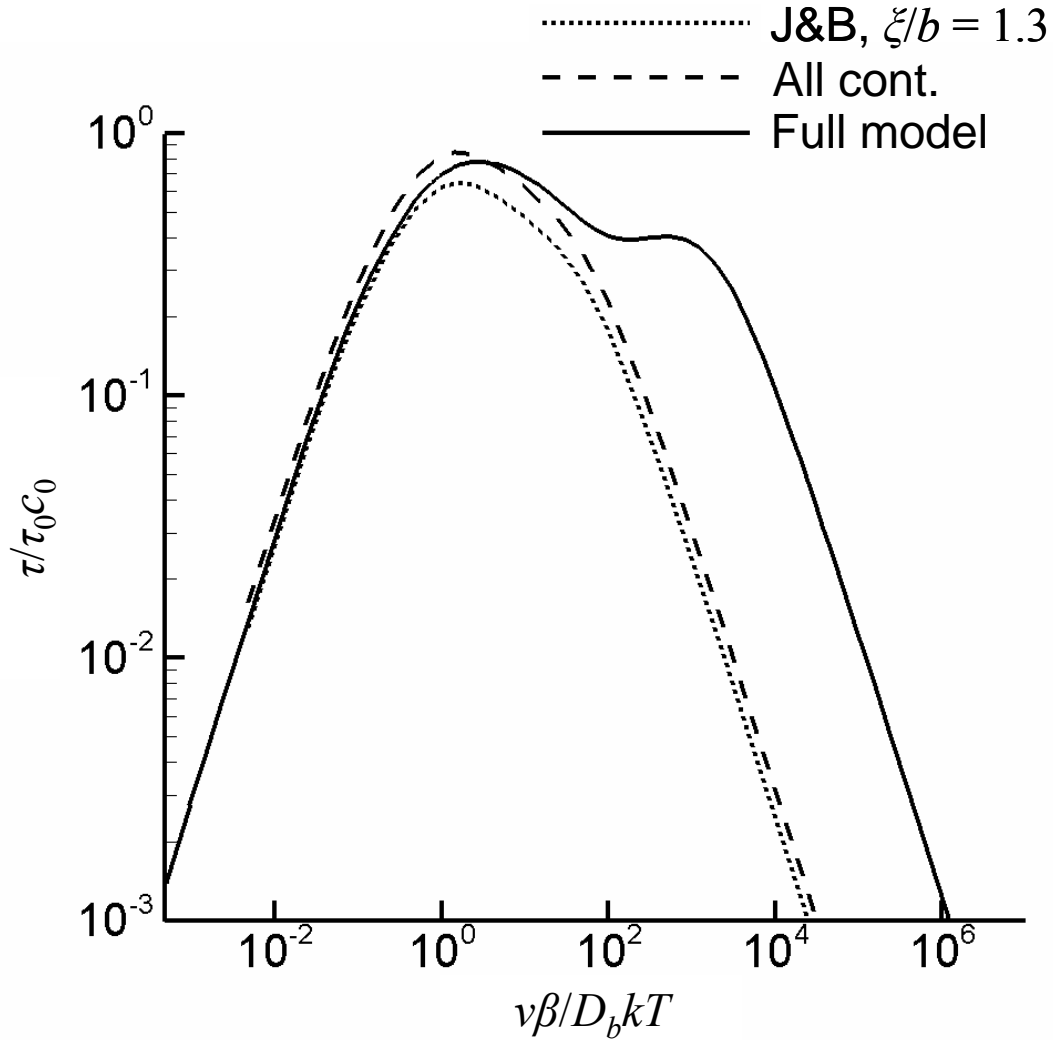


Figure 4. Normalized drag stress versus normalized dislocation velocity as predicted by three models. The ‘Full model’ uses the realistic core for Al. The ‘All cont.’ uses the solute enthalpy computed from the spread-core model of Eq. 10 in the domain including the core. The ‘J&B’ uses a solute enthalpy computed from the Peierls-Nabarro core with spreading parameter $\xi = 1.3b$ fit to best match the full model.

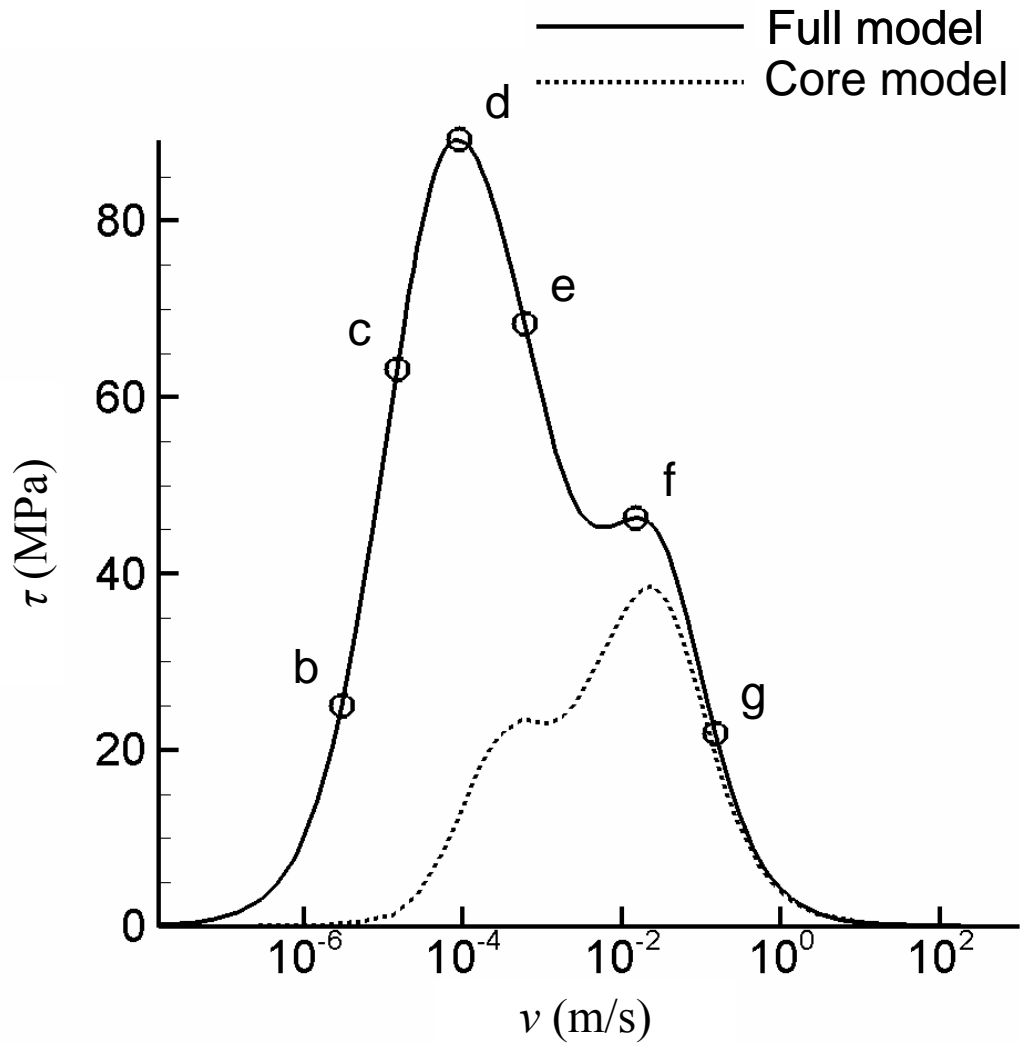


Figure 5. Shear stress vs dislocation velocity as predicted for the realistic edge dislocation core in Aluminum (solid curve). Also shown is the drag stress as predicted when only core diffusion processes are permitted (dotted curve). Circles denote points corresponding to the concentration distributions shown in figure 6.

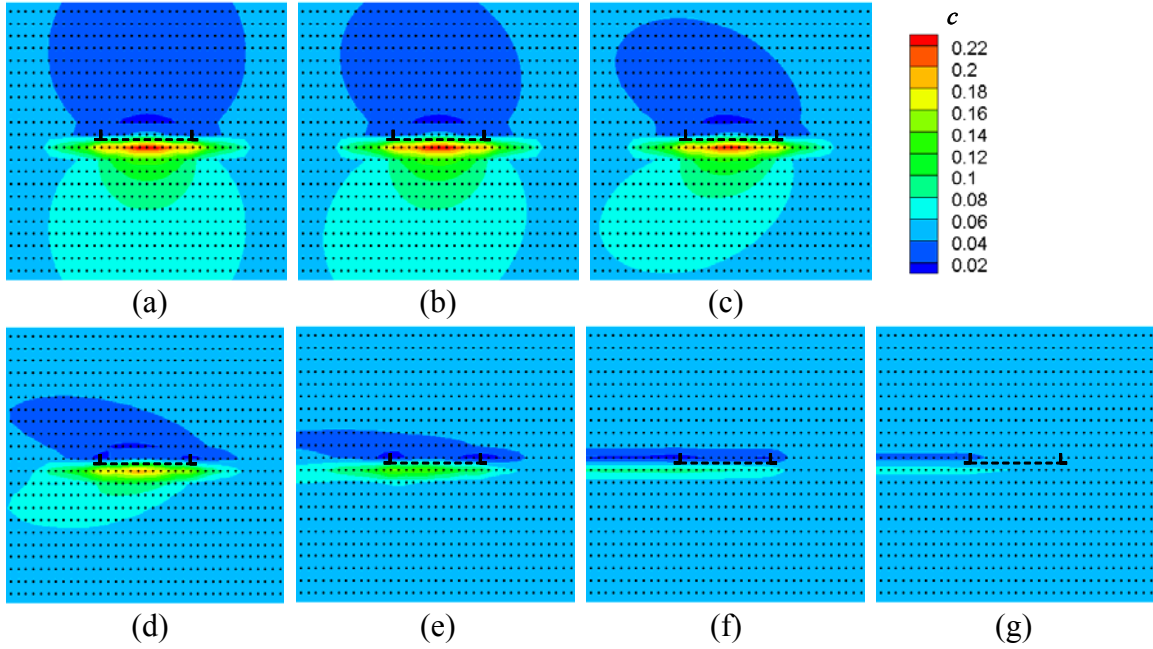


Figure 6. Solute concentration distribution around a moving dislocation for various velocities corresponding to the circled points in Figure 5: (a) $v = 0$ m/s; (b) $v = 2.98 \times 10^{-6}$ m/s; (c) $v = 1.49 \times 10^{-5}$ m/s; (d) $v = 8.95 \times 10^{-5}$ m/s; (e) $v = 5.97 \times 10^{-4}$ m/s; (f) $v = 0.0150$ m/s; (g) $v = 0.149$ m/s.

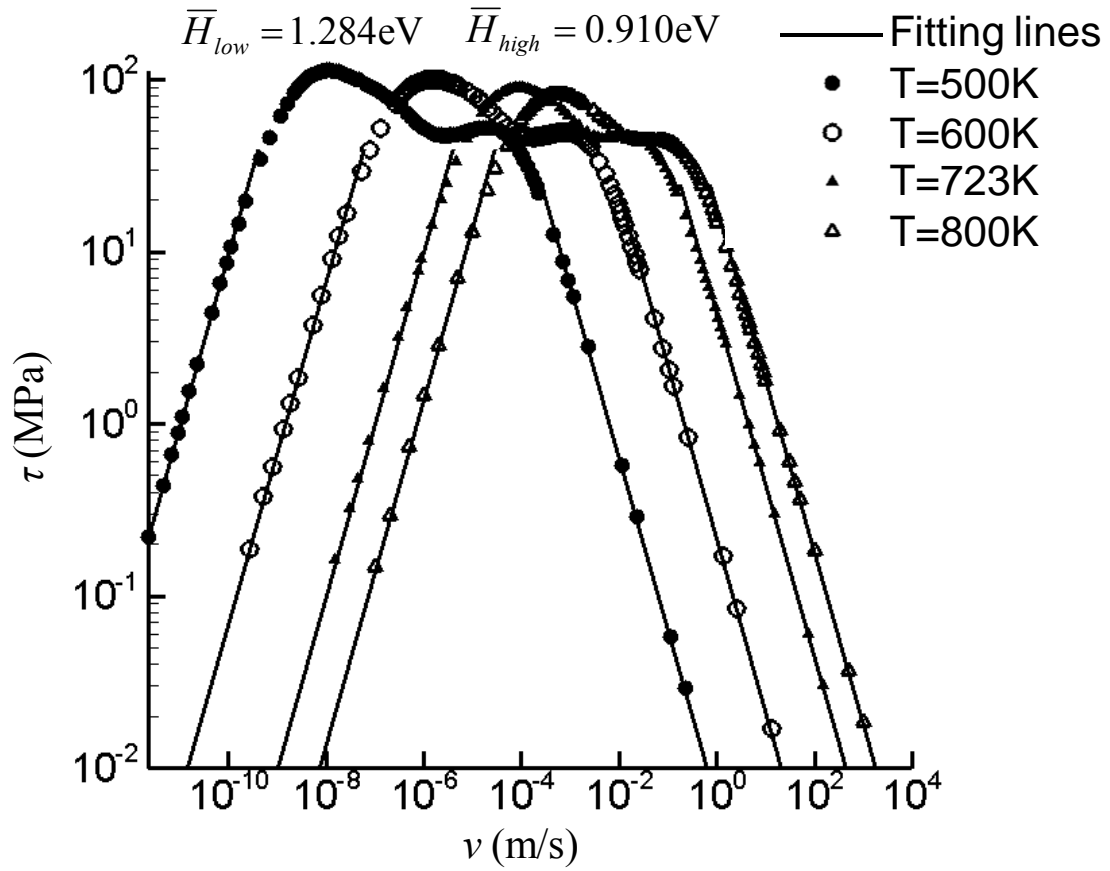


Figure 7. Shear stress vs velocity, on a logarithmic scale, for temperatures as indicated (symbols). The lines are linear fits to data at low and high velocities. Activation energies for the mechanisms in these regimes are indicated.

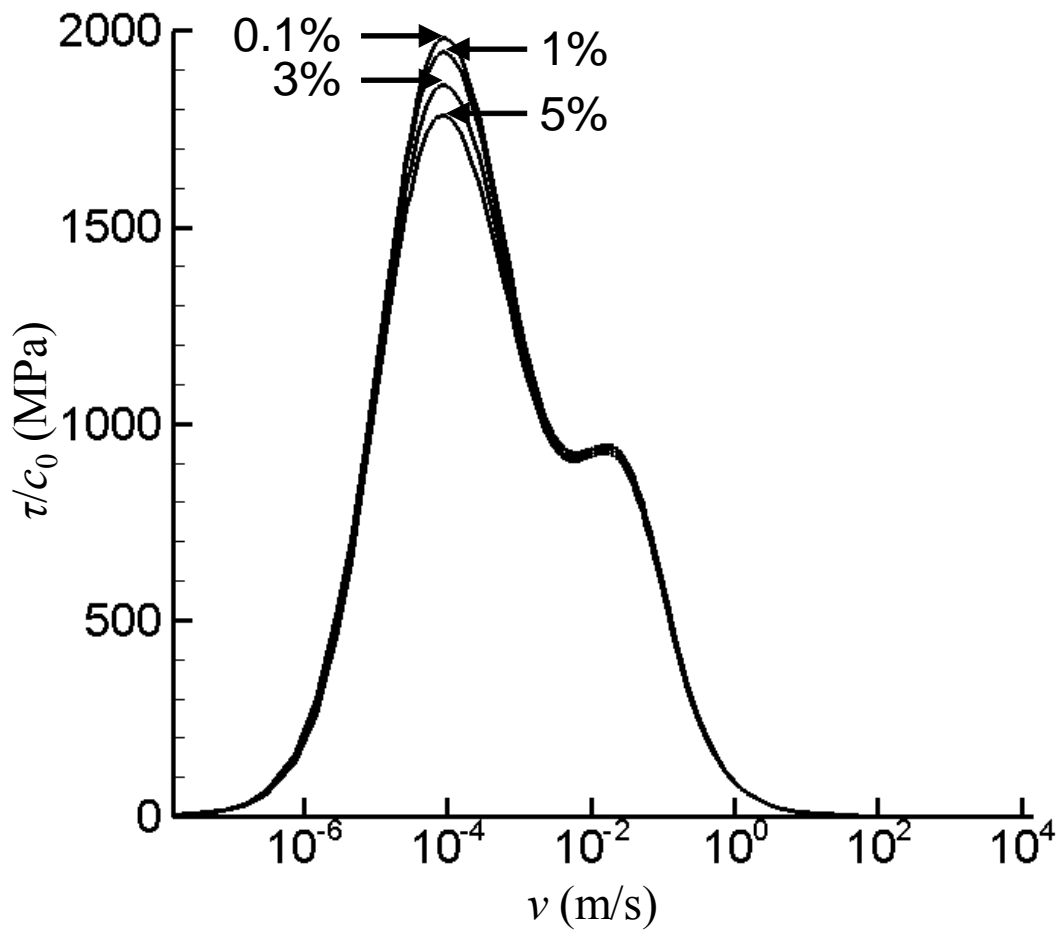


Figure 8. Shear stress normalized by the solute concentration vs velocity of dislocation for Al alloys with 0.1at%, 1at%, 3at% and 5at% Mg at T=723K.

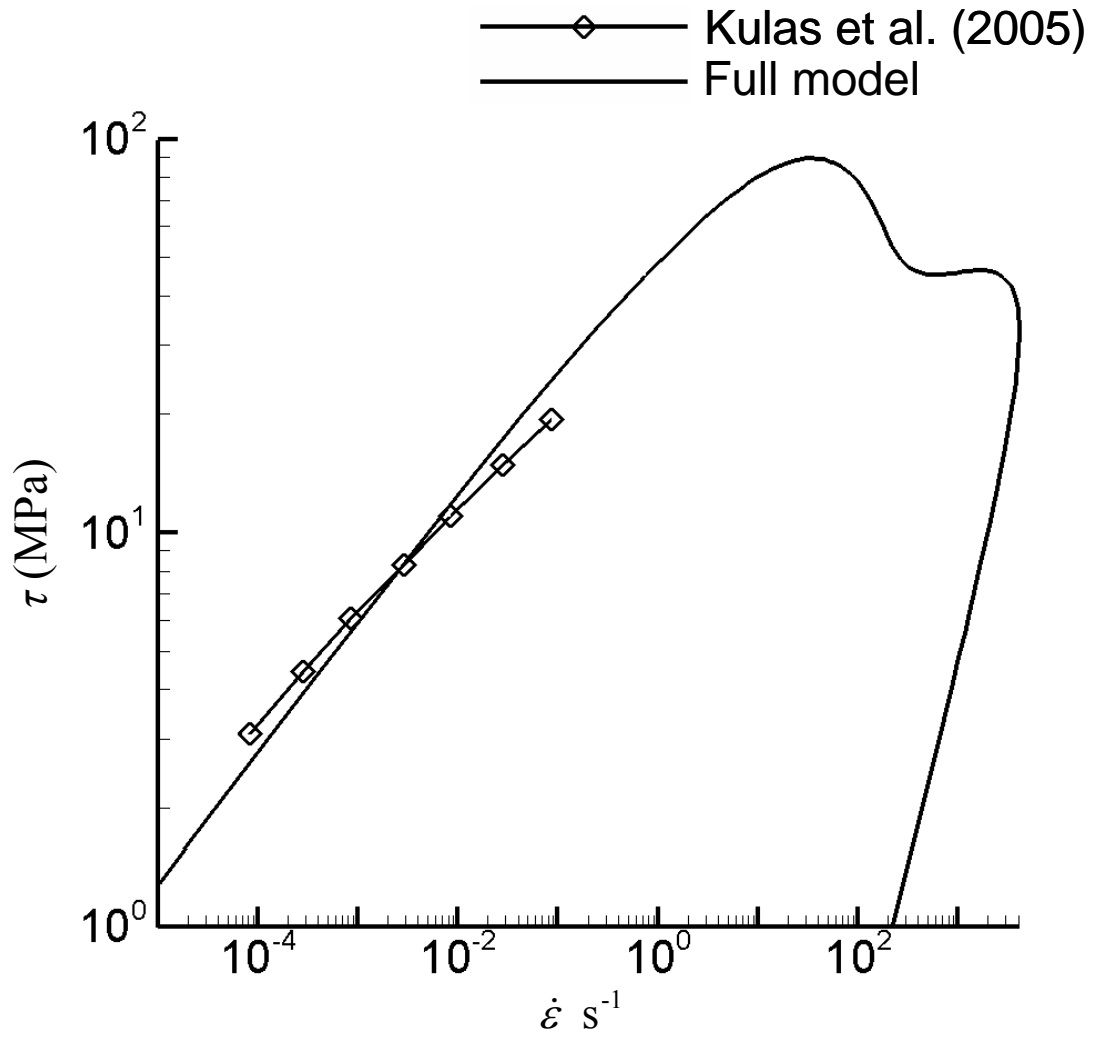


Figure 9. Shear stress vs shear strain rate curve as predicted by the current model of (20) using $\alpha = 0.322$ and as measured experimentally [23], for a temperature of 723K.